International Journal of Power Electronics and Drive Systems (IJPEDS)
Vol. 12, No. 3, September 2021, pp. 1832~1844
ISSN: 2088-8694, DOI: 10.11591/ijpeds.v12.i3.pp1832-1844

Generator and grid side converter control for wind energy conversion system

Asma Tounsi, Hafedh Abid
Laboratory of Sciences and Techniques of Automatic control & computer engineering (Lab-STA), National School of Engineering of Sfax ENIS, University of Sfax, Tunisia

Article Info

Article history:

Received Apr 4, 2021
Revised Jun 3, 2021
Accepted Jul 14, 2021

Keywords:

DC bus
Generator side converter
Grid side inverter
Permanent magnet synchronous Generator
Takagi-Sugeno
Wind energy conversion system

ABSTRACT

This paper focuses on the modeling and control of a wind energy conversion chain using a permanent magnet synchronous machine. This system behaves a turbine, a generator, DC/DC and DC/AC power converters. These are connected on both sides to the DC bus, where the inverter is followed by a filter which is connected to the grid. In this paper, we have been used two types of controllers. For the stator side converter, we consider the Takagi-Sugeno approach where the parameters of controller have been computed by the theory of linear matrix inequalities. The stability synthesis has been checked using the Lyapunov theory. According to the grid side converter, the proportional integral controller is exploited to keep a constant voltage on the DC bus and control both types of powers. The simulation results demonstrate the robustness of the approach used.

Corresponding Author:

Asma Tounsi
Laboratory (Lab-STA), ENIS
University of Sfax
Université de Route de l'Aéroport Km 0.5 BP 1169 .3029 Sfax Sfax, 3029, Tunisia
Email: asmatounsi130@gmail.com

1. INTRODUCTION

Wind energy (WE) is considered as the first sources exploited by humans after the energy of wood [1], [2]. It has been used to generate electrical energy for several decades [3], [4]. According to the renewable energies observatory, WE are at this time the most dynamic sector energy in the world [5]. Following the global oil crisis, the development and marketing of wind turbines was strongly encouraged [6]. Since then, the exploitation of wind resources has become increasingly efficient and the wind industry has experienced considerable growth over the last decade [7]. There exist two structures of wind turbines [3], [5]; the first structure operates at a fixed speed. It is directly connected to the electrical energy network. Whereas, the second structure operates at variable speed, this type of turbines can follow wind speed variations, such systems requiring power converters between generators and the grid.

Several types of generators can be used such as asynchronous machine, dual feed induction machine and permanent magnet synchronous generator (PMSG). Newly, the exploitation of the PMSG becomes more and more common thanks to its advantages. Indeed, the direct connection of the PMSG to the turbine allows to obtain a significant at reduced speed [7]. For small power wind turbines, the use of a PMSG avoids the use of the gearbox, while for big power wind turbines, a gearbox is needed despite the use of the PMSG. The latter is connected to a rectifier, which supplies a DC bus connected on the other side to an inverter. This allows to separate the controls of the converters of stator and grid sides. For stator side converter (SSC), many control

methods are used in the literature, such as field-oriented control approach [8], feedback linearization control [9], these controllers are simple but they are classical and lack performance. Other works used sliding mode control [10] and backstepping control [11] however their main drawbacks are the complexity and difficulty of implementation. Thus, to overcome the drawbacks of the controllers mentioned above and thanks to the advantages given by Takagi Sugeno (TS) fuzzy controller applied to nonlinear systems and which has proven its performance and efficiency, we used in this work the TS controller and we applied the theory of Lyapunov stability.

The aim of the control of grid side converter (GSC), makes it possible to control the production of active and reactive power as well as the maintenance of a constant voltage at the level of the DC bus [7]. In this part, we used the classical proportional integral (PI) controller thanks to its simplicity, so two control loops have been used in this section, an external control loop for the voltage of the DC bus, and an internal control loop for the powers. Thanks to the proportionality relationship between powers and currents, the power control is brought to a current control. So decoupling control of direct and quadrature currents is vital in order to control separetly the two types of powers [7].

The main contribution in this paper consists in using a TS fuzzy estimator and a TS fuzzy controller. The fuzzy estimator makes it possible, from any value of the wind speed, to predict the angular speed and the power converted at the level of the synchronous generator. While the TS fuzzy controller provides angular speed control, the electric power as well as the direct and quadrature currents of the synchronous generator.
The paper is structured as shown in: The second section presents a general overview of the WECC and models each component. Section 3 describes the controller used for each part of the chain. The results of simulation are given in section 4 to confirm effectiveness of controllers. The paper is closed by a conclusion.

2. WIND ENERGY CONVERSION CHAIN BASED ON PMSG

The wind energy conversion chain (WECC) is made up of two parts, the first is defined by a turbine, a generator and a rectifier, while the second is made up of a DC bus, an inverter and a filter which is connected to the grid. The conversion principle described above is illustrated by the Figure 1.

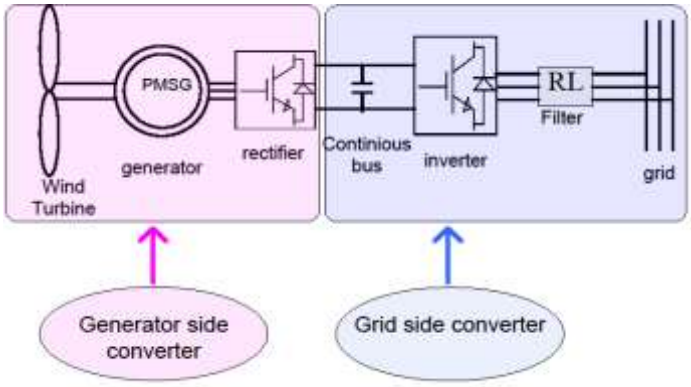

Figure 1. General structure of wind energy conversion chain

2.1. Wind turbine modeling

The turbine is the first component of the WECC, the latter tranforms kinetic energy into mechanical energy. The converted aerodynamic power from wind is defined as [12]-[14]:

$$P = \frac{1}{2} r_o \pi R^2 C_p(\lambda) V^3 \quad (1)$$

Where r_o, C_p, R, V and represent respectively the air density, the power coefficient, the length of the blade and the wind speed.The power coefficient is characterized by [15], [16]:

$$C_p(\lambda, \beta) = 0.5176 \left(116 \frac{1}{\lambda_i} - 0.4\beta - 5\right) e^{\frac{-21}{\lambda_i}} + 0.0068\lambda \quad (2)$$

Where λ_i is described by as shown in [17] ,[18]:

$$\frac{1}{\lambda_i} = \frac{1}{\lambda + 0.08\beta} - \frac{0.035}{\beta^3 + 1} \quad (3)$$

The expression of tip speed ratio λ is [18]:

$$\lambda = \frac{\Omega R}{V} \quad (4)$$

Where, Ω represents the mechanical rotation speed. The overall mechanical dynamics of WECC is given by the as shown in [15], [19]:

$$J\frac{d\Omega}{dt} = T_m - T_{em} - f\Omega \quad (5)$$

Where *J* represents the global inertia moment which depends on the turbine inertia, the generator inertia and the gearbox reduction.

2.2. PMSG modeling

The turbine is followed by a PMSG. From this machine, we obtain electrical energy. The electromagnetic torque of the machine in the d-q rotating frame is expressed as [20]:

$$T_{em} = \frac{3}{2}p[\phi_f I_{s.q} + (L_{s.d} - L_{s.q})I_{s.d}I_{s.q} \quad (6)$$

For the PMSG we consider that [10]:

$$L_{s.d} = L_{s.q} = L_S \quad (7)$$

So,

$$T_{em} = \frac{3}{2}p\phi_f I_{s.q} \quad (8)$$

The dynamics behavior of the PMSG can be modeled by the as shown of state [21] :

$$\dot{x}(t) = Ax(t) + Bu(t) \quad (9)$$

Where *A* represents the state matrix, *B* the control vector, *x* describes the state vector and *u* is the control input. The state vector and the control input are respectively defined as:

$$x(t) = [i_{s.d} \quad i_{s.q} \quad \Omega]^T, u = [V_{s.d} \quad V_{s.q}]^T$$

$$A = \begin{pmatrix} -\frac{R_S}{L_S} & P\Omega & 0 \\ -P\Omega & -\frac{R_S}{L_S} & \frac{P\phi_f}{L_S} \\ 0 & \frac{-3P\phi_f}{2J} & -\frac{f}{J} \end{pmatrix}$$

The state matrix *A* includes the angular velocity Ω. However, the TS fuzzy model includes two local models each one is characterized by the state matrix A_i.

$$A_1 = \begin{pmatrix} -\frac{R_S}{L_S} & P\Omega_{min} & 0 \\ -P\Omega_{min} & -\frac{R_S}{L_S} & \frac{P\varphi_f}{L_S} \\ 0 & \frac{-3P\varphi_f}{2J} & -\frac{f}{J} \end{pmatrix}, A_2 = \begin{pmatrix} -\frac{R_S}{L_S} & P\Omega_{max} & 0 \\ -P\Omega_{max} & -\frac{R_S}{L_S} & \frac{P\varphi_f}{L_S} \\ 0 & \frac{-3P\varphi_f}{2J} & -\frac{f}{J} \end{pmatrix}$$

The TS fuzzy model of the system can be described by if-then rules.

$$\textit{Rule } i\text{: If} \quad z(t) \textit{ is } F_i \qquad \textit{Then} \quad \dot{x}(t) = A_i x(t) + Bu(t) \quad \textit{for } i = 1,2 \quad (10)$$

The member ship functions are chosen as rectangular form, which nonlinearity is presented by two models:

$$F_1 = \frac{\Omega - \Omega_{min}}{\Omega min_{max}} \quad (11)$$

$$F_2 = 1 - F_1 = \frac{\Omega_{max}}{\Omega min_{max}} \quad (12)$$

The TS fuzzy model can be written as [22], [23]:

$$\dot{x}(t) = \sum_{i=1}^{r} \mu_i\big(z(t)\big)\big(A_i x(t) + Bu(t)\big) \quad (13)$$

Where, *r* is the rule's number (number of linear local model). The activation's degree for rule is defined as:

$$\mu_i(z(t)) = \frac{F_i}{\sum_{j=1}^{r} F_j}, 0 \prec \mu_i(z(t)) \prec 1, i = 1, \ldots r$$

2.3. Grid side inverter modeling

The two parts of WECS are linked through a continuous bus as shown by Figure 2. The modeling of the second part of the chain is given by these different equations [24]:

$$V_{g.d} = V_d - R_f i_{g.d} - L_f \frac{di_{g.d}}{dt} + \omega_g L_f i_{g.q} \quad (14)$$

$$V_{g.q} = V_q - R_f i_{g.q} - L_f \frac{di_{g.q}}{dt} + \omega_g L_f i_{g.d} \quad (15)$$

$$C \frac{dU_{dc}}{dt} = I_{dc.s} - I_{dc.g} \quad (16)$$

Where $(V_{g.d}, V_{g.q})$ are grid voltages of d-q axes, (V_d, V_q) designate the direct and quadrature components of the output inverter, $(I_{g.d}, I_{g.q})$ represent the grid currents along d and q axes, R_f and L_f represent respectively the resistance and the inductance of the filter, ω_g represents the angular frequency, C is the capacitance of the capacitor, U_{dc} represents the DC voltage of the capacitor, $I_{dc.s}$ is the current of the SSC output to the DC link and $I_{dc.g}$ is the current of the DC link output to the grid. The following two equations represent respectively the formulas relating to the active and reactive power [18]:

$$P = V_{g.d} i_{g.d} + V_{g.q} i_{g.q} \quad (17)$$

$$Q = V_{g.q} i_{g.d} - V_{g.d} i_{g.q} \quad (18)$$

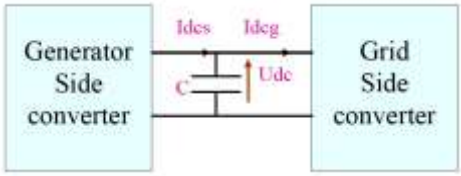

Figure 2. DC link capacitor

3. CONTROL STRATEGIES OF THE WIND SYSTEM

In this section, we are interested in controlling the WECS. It has two parts, the first relates to the control of the SSC and the second relates to the control of the GSC.

3.1. Controller for generator side converter

To maximize the conversion of wind energy, some equations of the system are used. The power coefficient is keeped at its maximum value Cpmax as well as the optimum value of the tip speed ratio. Likewise, mechanical rotational speed Ω must be maintained at an optimum value and vary proportionally with the wind speed *V*. So, the mechanical reference speed is expressed as:

$$\Omega_{ref} = \frac{\lambda_{opt} V}{R} \quad (19)$$

The power extracted by the wind turbine is also maintained at its maximum and it is expressed as shown in:

$$P \frac{1}{2_o} 5 \frac{\Omega_{ref}{}^3}{\lambda_{opt}{}^3} {}_{pmax_{max}} \quad (20)$$

The direct reference current is equal to zero and the q-axis reference current is obtained based as shown in (10):

$$I_{s.qref} = \frac{2}{3} \frac{T_{emref}}{p\phi_f} \quad (21)$$

It is indispensable to control the mechanical speed of the turbine blades as well as the currents of the generator to increase the efficiency of the energy transformation. The diagram of the control strategy is presented in Figure 3, which includes two fuzzy blocks. The first block is a Takagi-Sugeno fuzzy estimator while the second is the Takagi Sugeno fuzzy controller.

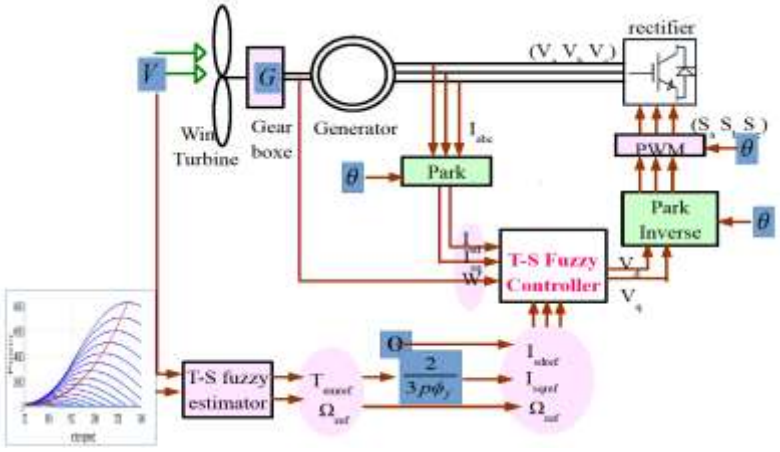

Figure 3. Stator side converter control

3.1.1. T-S Fuzzy estimator

Based on the minimum and maximum wind speeds *(V_{min}, V_{max})* allowed by the turbine as well as the corresponding optimum angular speed *(Ω_{opt1}, Ω_{opt2})* to each of these wind speeds and the corresponding optimum power. It is then possible to predict, using a TS type fuzzy supervisor, the optimal angular speed Ω_{opt} and the electrical power generated P_{opt} for any wind speed located in the *(V_{min}, V_{max})* range. Membership functions are shown in Figure 4.

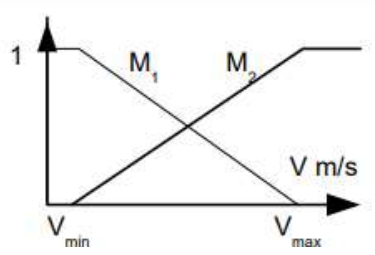

Figure 4. Membership function

$$\Omega_{ref} = \Omega_{opt} = M_1 \Omega_{opt1} + M_2 \Omega_{opt2} \quad (22)$$

$$P_{ref} = P_{opt} = N_1 P_{opt1} + N_2 P_{opt2} \quad (23)$$

Where, $N_1 = \frac{V^3 - V_{min}^3}{V_{max}^{3\,min}}$, $N_2 = \frac{V_{max}^3}{V_{max}^{3\,min}}$ denote the member ship function for power extraction,

$P_{opt1} and P_{opt2}$ denote the optimum power for the maximum and minimum wind speed respectively.

3.1.2. TS type fuzzy controller

To control speed and stator current, we propose parallel-distributed compensation (PDC) controller, which is based on TS fuzzy theory. The PDC controller has been proposed to stabilize the nonlinear system. The PDC controller rules can be written in the form:

Rule: if $z_1(t)$ is F_{1i} and $z_p(t)$ is F_{pi}, so $u(t) = - k_i x(t)$ $i=1,...,r$

Which is a state feedback controller to the consequence part. The TS fuzzy controller is expressed by:

$$u(t) = -\sum_{i=1}^{r} \mu_i\big(z(t)\big) K_i x(t) \quad (24)$$

With k_i represents the gain for local model for $i=1,..,r$. The following expression defined the tracking error:

$$e_r(t) = x(t) - x_{ref}(t) \quad (25)$$

The derivate expression is expressed by:

$$\dot{e}_r = \dot{x} - \dot{x}_{ref} \quad (26)$$

In a tracking problem, the expression of the control law (24) becomes as shown in [9]:

$$u(t) = -\sum_{i=1}^{2} \mu_i\big(z(t)\big) K_i e_r(t) \quad (27)$$

So,

$$\dot{e}_r = \sum_{i=1}^{2} \mu_i\big(z(t)\big) (A_i e_r + Bu) \quad (28)$$

$$\dot{e}_r = \sum_{i=1}^{2}\sum_{j=1}^{2} \mu_i \mu_j \left(A_i e_r - B k_j e_r\right) = \sum_{i=1}^{2}\sum_{j=1}^{2} \quad \mu_i\mu_j \left(A_i - B k_j\right) e_r \quad (29)$$

Theorem:

The error of the overall closed loop system converge to zero, if there exists a matrix X definite positive which satisfies the following matrix inequalities:

$$X A_i^T + A_i X - M_i^T B^T - B M_i \prec 0, \; i=1..r \quad (30)$$

$$X A_i^T + A_i X + X A_j^T + A_j X - M_j^T B^T - M_i^T B^T - B M_j - B M_i \prec 0, \; i<j=<r \quad (31)$$

Where $\boldsymbol{M_i = K_i X}$ and $\boldsymbol{X = P^{-1}}$

Proof:

The quadratic Lyapunov candidate function is chosen as follows:

$$V(e_r) = e_r^T P e_r \quad (32)$$

Where, e_r is the error and P is the symmetric matrix definite positive. The derivate of the Lyapunov function is:

$$\dot{V}(e_r) = \dot{e}_r^T P e_r + e_r^T P \dot{e}_r \quad (33)$$

Using as shown in (29), its follows that:

$$\dot{V} = \left(\sum_{i=1}^{2}\sum_{j=1}^{2} \mu_i \mu_j \left(A_i - B K_j\right) e_r\right)^T P e_r + e_r^T P \left(\sum_{i=1}^{2}\sum_{j=1}^{2} \mu_i \mu_j \left(A_i - B K_j\right) e_r\right) \quad (34)$$

$$\dot{V} = \sum_{i=1}^{2}\sum_{j=1}^{2}\mu_i\,\mu_j\left({e_r}^T\left(A_i - BK_j\right)^T P e_r + {e_r}^T P\left(A_i - BK_j\right)e_r\right) \quad (35)$$

$$\dot{V} = \sum_{i=1}^{2}\sum_{j=1}^{2}\mu_i\,\mu_j\left({e_r}^T\left(\left({A_i}^T - {K_j}^T B^T\right)P + P\left(A_i - BK_j\right)\right)e_r\right) \quad (36)$$

$$\dot{V} = \sum_{i=1}^{2}\sum_{j=1}^{2}\mu_i\,\mu_j\left({e_r}^T\left({A_i}^T P - {K_j}^T B^T P + PA_i - PBK_j\right)e_r\right) \quad (37)$$

to prove that as shown in (37) is negative we transform the stability problem into LMI problem.

$$\dot{V} = \sum_{i=1}^{2}{\mu_i}^2\left({e_r}^T\left({A_i}^T P - {K_i}^T B^T P + PA_i - PBK_i\right)e_r\right) + \sum_{i=1}^{2}\sum_{j=1}^{2}\mu_i\,\mu_j\left({e_r}^T\left({A_i}^T P + {A_j}^T P + PA_i + PA_j - {K_j}^T B^T P - {K_i}^T B^T P - PBK_j - PBK_i\right)e_r\right) \quad (38)$$

It is very clear that as shown in (38) is a bilinear matrix inequality (BLMI). However, to transform as shown in (38) into an LMI, we must multiply the inequality in the left and the right by P^{-1}. Then we make the following change of variable $X = P^{-1}$. Then we obtain theas shown in:

$$\dot{V} = \sum_{i=1}^{2}{\mu_i}^2\left({e_r}^T\left(X{A_i}^T - {M_i}^T B^T + A_i X - BM_i\right)e_r\right) + \sum_{i=1}^{2}\sum_{j=1}^{2}\mu_i\,\mu_j\left({e_r}^T\left(X{A_i}^T + X{A_j}^T + A_i X + A_j X - {M_j}^T B^T - {M_i}^T B^T - BM_j - BM_i\right)e_r\right) \quad (39)$$

with $M_i = K_i X$

We remarque that as shown in (39) is the sum of two terms. To guarantee that this latter is negative. Each term must be negative. However, we get the following equations which verify the proposed theorem.

$$X{A_i}^T + A_i X - {M_i}^T B^T - BM_i \prec 0,\ i=1r \quad (40)$$

$$X{A_i}^T + A_i X + X{A_j}^T + A_j X - {M_j}^T B^T - {M_i}^T B^T - BM_j - BM_i \prec 0,\ i<j\leq r \quad (41)$$

$$\dot{V}(e_r) = {\dot{e}_r}^T P e_r + {e_r}^T P\dot{e}_r \quad (42)$$

So,

$$\dot{V}(e_r) \leq 0 \quad (43)$$

3.2. Controller of grid side converter

In this part, we are interested to control the DC voltage across DC bus and powers, which will be transmetted to power grid. According to as shown (17) and (18), the two powers previously defined are strongly coupled, which makes it difficult to control them independently. However, it is necessary to decouple them. For this, we choose to align the direct axis component of the grid voltage with the direct axis of the field-oriented control frame and we keep zeroing the componen of grid voltage along the quadrature axis [25].

$$V_{gq} = 0 \quad (44)$$

$$V_{gd} = V_g \quad (45)$$

Therefore, the powers equations become as shown in [25]:

$$P = V_g i_{gd} \quad (46)$$

$$Q = -V_g i_{gq} \quad (47)$$

Therefore, the expressions of these two powers are decoupled as shown (46) and (47). The currents along the direct and quadrature axes allow to controlrespectively the active and reactive powers. Figure 5 describes the diagram structure of the current controllers along the d and q axes.

(a) (b)

Figure 5. (a) currents control along d-axis, and (b) currents control along q-axis

The transfert function of the open loop is given by :

$$H_{OL} = \frac{K_i+K_pS}{S}\frac{1}{(L_fS+R_f)} \quad (48)$$

To determine the parameters of the PI controller, we use the pole compensation method. However, we choose

$K_p = L_f$ And $K_i = 20R_f$

So, the transfer function in closed loop becomes as:

$$H_{CL} = \frac{1}{\tau S+1} \quad (49)$$

where, $\tau = \frac{R_f}{K_i} = 0.05$

We propose a PI type controller to keep a constant DC bus. In this case, two control loops are obtained along the direct axis. A first internal loop for controlling the current and a second external loop for the voltage of DC bus. In this case, the reference current along the direct axis is provided by the output of the controller. Figure 6 describes the general structure of the DC bus voltage controller.

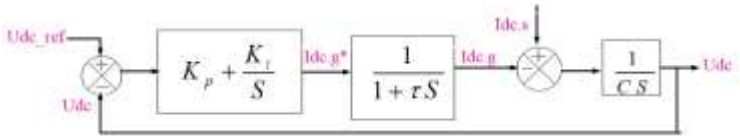

Figure 6. General structure for DC bus control

The current transfer function represents a first order function, where $\tau \prec\prec 1$. However, we approximate the function to a unit gain, so the transfer function of open loop of the DC bus voltage can be written as:

$$H_{OL} = (K_p + \frac{K_i}{S})\frac{1}{CS} \quad (50)$$

The transfer function of closed loop is presented by:

$$H_{CL} = \frac{\frac{K_p}{K_i}S+1}{\frac{C}{K_i}S^2+\frac{K_p}{K_i}S+1} \quad (51)$$

This function is of the form:

$$H = \frac{1}{\frac{1}{{\omega_0}^2}S^2+\frac{2\xi}{\omega_0}S+1} \quad (52)$$

With ξ describes the damping factor and ω_0 represents the own pulsation of the system. In this work $\xi=1$ and $\omega_0=40$ *rad/s*. Finally, we obtain the parameters of the DC bus controller:

$$K_i = C\omega_0{}^2 \quad (53)$$

$$K_p = 2\xi C\omega_0 \quad (54)$$

Figure 7 summarizes the GSC control part, indeed, the measured currents are compared to their references. The direct reference current is obtained from the DC bus controller, while the quadrature reference current is zero to obtain zero reactive power. Two PI controllers are proposed, one for direct current and the other for quadrature current. The compensation terms are added to the voltages obtained at the output of these two controllers. The two finally obtained voltages are transformed by the PARK transformation to obtain the modulating voltages which will be compared with a carrier: this is the principle of pulse width modulation (PWM).

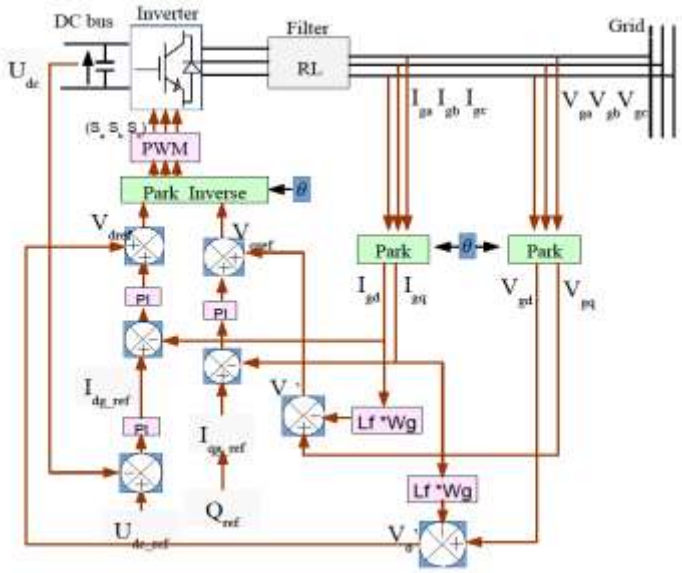

Figure 7. Grid side inverter control

4. RESULTS OF SIMULATION

In order to chek the performance of the controllers, some results obtained are presented in this section. For this, the system parameters used are given in Table 1, Table 2 and Table 3.

Table 1. Turbine parameters

Radius of blades	Tip speed ratio	Pitch Angle	Rated power
R = 3 m	λ_{opt}=8.1	β = 0	P=10 Kw

Table 2. PMSG parameters

Inertia	Friction coefficient	Stator resistance	d-q axis inductance	Magnetic flux	Number of poles pair	Gearbox
J = 0.05 N.m	F = 0.006 Nm sec/rad	R_s = 0.5 Ohm	L_s = 1 Mh	Φ_f = 0.16 wb	P = 8	G=8

Table 3. DC bus parameters

Capacitor	Udc_ref
10e-4 F	400 V

The resolution of the LMIs (30) and (31) gave the following matrix X and gains K_i:
X= *[0.3230 -0.0000 0.0000; -0.0000 0.3284 -0.6670; 0.0000 -0.6670 58.4888]*
K_1= *[1.1295 -67.3718 136.8268; 66.2580 1.0497 5.7163]*

K_2= *[1.1295 -111.1048 225.6451; 109.2680 1.0497 5.7163]*
K_3 = *[1.1295 -133.3102 270.7425; 131.1063 1.0497 5.7163]*
K_4 = *[1.1295 0.0089 -0.0180; -0.0087 1.0497 5.7163]*
The parameters of the PI controllers have been chosen as:
For the currents: K_p=*0.05* and K_i=*10*
For the DC bus voltage: K_p=*0.8* and K_i=*16*

The real wind speed can take any value, for this work we chose as shown in curve Figures 8 to10. The power coefficient reaches its maximum and it is maintained at this value despite the change of wind speed as given in the Figure 9. This coefficient guarantees the extraction of the optumum power as described in Figure 10, in fact the power is maintained at the maximum value for the two values of the wind thanks to the best value of power coefficient.

The angular speed is given by Figure 11. It is clear that the measured angular speed follows the reference angular speed even when changing the wind speed. The evolution in the behavior of the currents along the axes q and d is presented in Figures 12 and 13. It is clear that the curves obtained by the controller follow the reference curves. In fact, the current obtained along the q-axis is near to its reference in the two wind intervals. Also, the current along the d-axis is near to zero in both intervals.

Figure 14 demonstrates that the voltage across the DC bus is continuous and practically constant despite the change of the wind speed. The voltage value follows its reference. Figures 15 and 16 describe the obtained currents along axes d-q of the power grid side, these currents are near to the reference ones. The d-axis current follows its reference with a small overshoot when changing the wind speed. Also, the current along q-axis converge to zero.

Figure 17 represents the currents obtained at the output of the filter. These currents are three-phase, balanced and offset by 2*π/3. Their amplitude is influenced by the change of the wind speed, in fact they have the same appearance, and this is clarified in Figure 18 which we zoomed in for the two wind intervals to show the amplitude of the current in these two intervals.

Figure 19 represents the voltages obtained at the output of the filter. These voltages are three phases, balanced and offset by 2*π/3 and their amplitude is constant despite the change of the wind speed, this is clarified in Figure 20. Figure 19 represents the voltages obtained at the output of the filter. These voltages are three phases, balanced and offset by 2*π/3 and their amplitude is constant despite the change of the wind speed, this is clarified in Figure 20.

Figures 21 and 22 demonstrate that the two powers previously defined follow their references. In fact, the active power is near to its reference with a fairly small delay while the reactive power is practically zero. The tracking of powers to their references is due to the proportionality relationship between the currents and the powers and confirms the performance of the controller applied for control of the currents.

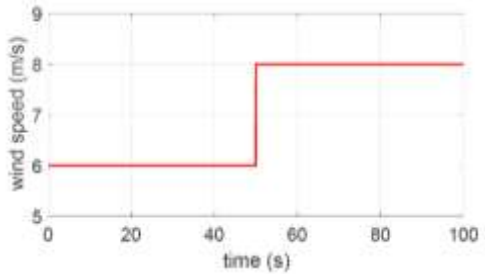

Figure 8. Evolution of wind speed

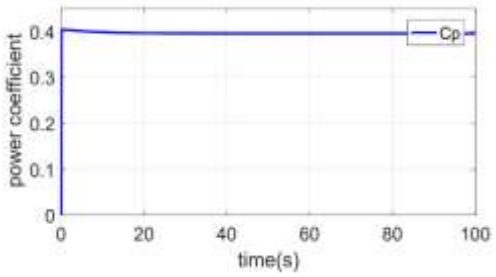

Figure 9. Power coefficient response

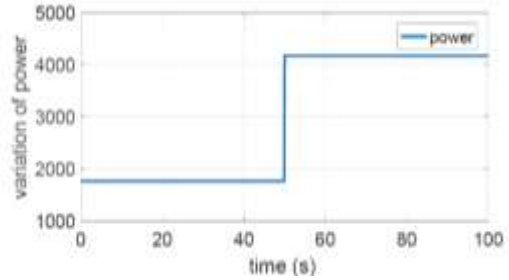

Figure 10. Evolution of power

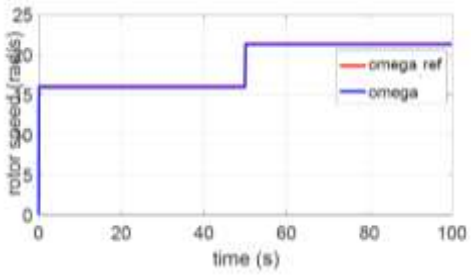

Figure 11. Angular speed

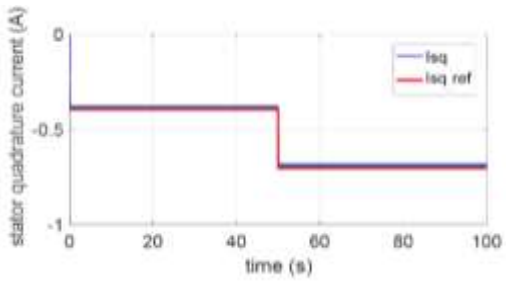

Figure 12. behaviour of Q-axis current

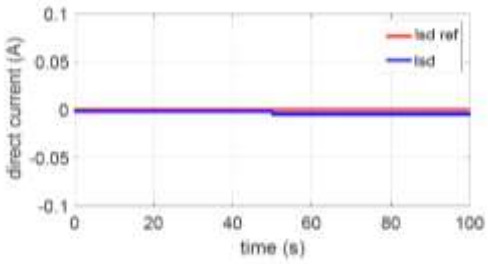

Figure 13. Behavior of D-axis current

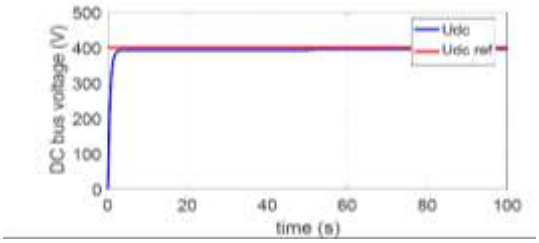

Figure 14. DC bus voltage

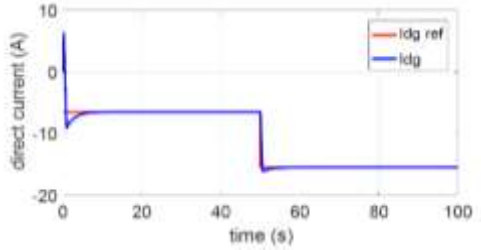

Figure 15. Grid-side direct current

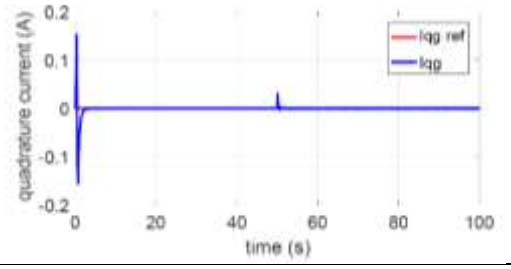

Figure 16. Grid-side quadrature current

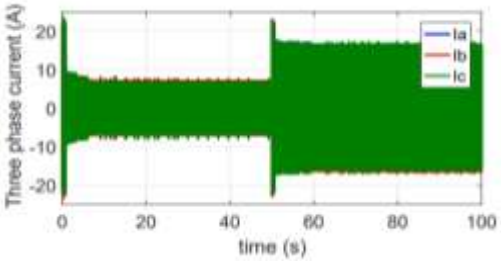

Figure 17. 3-phase current at the filter output

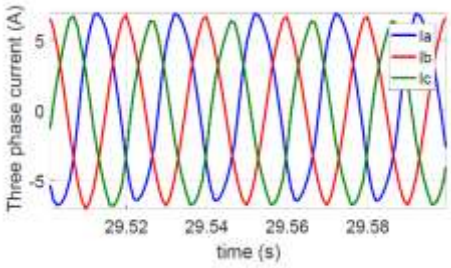

(a)

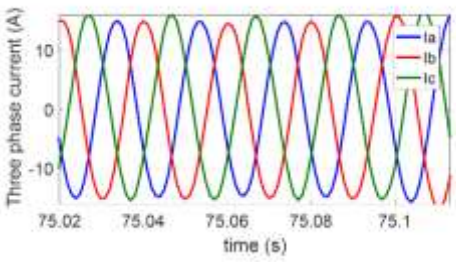

(b)

Figure 18. (a) zoom on currents for the first interval; (b) zoom on currents for the second interval

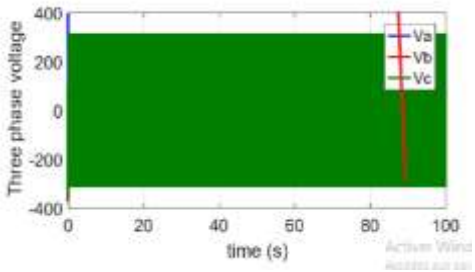

Figure 19. 3-phase voltage at the filter output

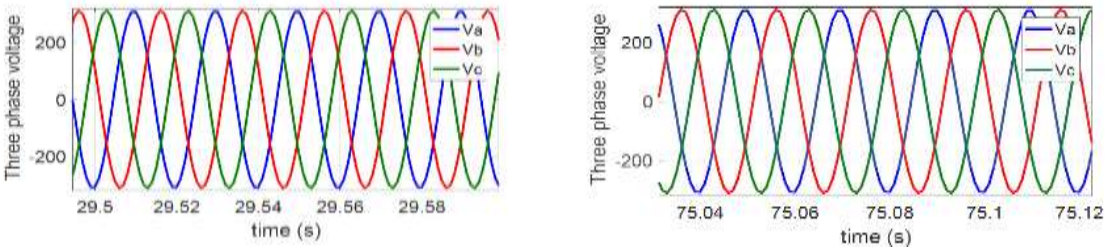

(a) (b)

Figure 20. (a) zoom on the voltages for the first interval; (b) zoom on the voltages for the second interval

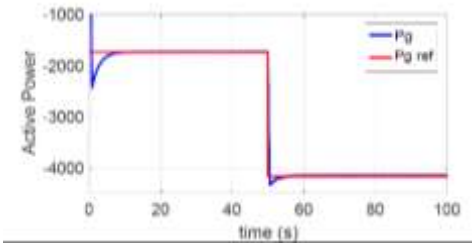

Figure 21. Active power

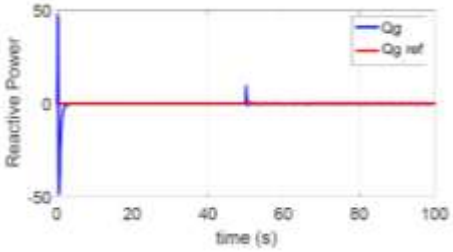

Figure 22. Reactive power

5. CONCLUSION

In this paper, we are concerned into control the WECC. However, we started with the modeling of the system. The latter has two parts, a first is called SSC and a second is called GSC. In the first part we have used a fuzzy estimator and a Takagi Sygeno type controller to maximize the conversion of wind energy. The fuzzy estimator makes it possible to predict the optimum mechanical rotation speed of the blades as well as the optimum power that the turbine can transform from the wind. In the second part, we have used a PI type controller. The goal is to retain the DC bus constant as well as the control powers. The results of simulation are given to demonstrate the performance of the proposed controllers in the two parts. It can be concluded that the two controllers have succeeded in achieving the desired objectives.

REFERENCE

[1] I. Yasmine, and B. B. Bekkali Chakib, "Power control of DFIG-generators for wind turbines variable-speed," *International Journal of Power Electronics and Drive Systems (IJPEDS)*, vol. 8, no. 1, pp. 444-453, Mar. 2017, doi: 10.11591/ijpeds.v8.i1.pp444-453.

[2] D. Ounnas, M. Ramdani, S. Chenikher, and T. Bouktir, "Optimal reference model based fuzzy tracking control for wind energy conversion system. *International Journal of Renewable Energy Research (IJRER)*, vol. 6, no. 3, pp. 1129-1136, 2016.

[3] H. Matayoshi, A. M. Howlader, M. Datta, and T. Senjyu, "Control strategy of PMSG based wind energy conversion system under strong wind conditions," *Energy for Sustainable Development*, vol. 45, pp. 211-218, Aug. 2018, doi: 10.1016/j.esd.2018.07.001.

[4] V. Meenakshi, and S. Paramasivam, "Control strategy used in DFIG and PMSG based wind turbines an overview," *International Journal of Power Electronics and Drive Systems (IJPEDS)*, vol. 8, no. 3, pp. 1160-1167, Sep. 2017, doi: 10.11591/ijpeds.v8.i3.pp1160-1167.
[5] F. Senani, A. Rahab, and H. Benalla, "A complete modeling and control for wind turbine based of a doubly fed induction generator using direct power control," *International Journal of Power Electronics and Drive Systems (IJPEDS)*, vol. 8, no. 4, pp. 1954-1962, Dec. 2017, doi: 10.11591/ijpeds.v8.i4.pp1954-1962.
[6] K. B. Tawfiq, A. S. Mansour, H. S. Ramadan, M. Becherif, and E. E. El-kholy, "Wind energy conversion system topologies and converters: comparative review," *Energy Procedia*, vol. 162, pp. 38-47, Apr. 2019, doi: 10.1016/j.egypro.2019.04.005.
[7] Y. Errami, M. Ouassaid, and M. Maaroufi, "A performance comparison of a nonlinear and a linear control for grid connected PMSG wind energy conversion system." *International Journal of Electrical Power & Energy Systems*, vol. 68, pp. 180-194, Jun. 2015, doi: 10.1016/j.ijepes.2014.12.027.
[8] S. Li, T. A. Haskew, and L Xu, "Conventional and novel control designs for direct driven PMSG wind turbines, *Electric Power Systems Research*, vol. 80, no. 3, pp. 328-338, Mar. 2010, doi: 10.1016/j.epsr.2009.09.016.
[9] Y. Lee, and Y. B. Shtessel, "Comparison of a feedback linearization controller and sliding mode controllers for a permanent magnet stepper motor," in *Proceedings of 28th Southeastern Symposium on System Theory*, Jan. 1996, doi: 10.1109/SSST.1996.493510.
[10] M. E. Emna, K. Adel, and M. F. Mimouni, "The wind energy conversion system using PMSG controlled by vector control and SMC strategies," *International Journal of Renewable Energy Research*, vol. 3, no. 1, pp. 41-50, Jan. 2013.
[11] M. Ayadi, and N. Derbel, "Nonlinear adaptive backstepping control for variable-speed wind energy conversion system-based permanent magnet synchronous generator," *The International Journal of Advanced Manufacturing Technology*, vol. 92, no. 1-4, pp. 39-46, Sep. 2017, doi: 10.1007/s00170-017-0098-3.
[12] S. Boubzizi, H. Abid, A. El hajjaji, and M. Chaabane, "Comparative study of three types of controllers for DFIG in wind energy conversion system," *Protection and Control of Modern Power Systems*, vol. 3, no. 1, pp. 1-12, doi: 10.1186/s41601-018-0096-y.
[13] V. Sekhar, "Modified fuzzy logic based control strategy for grid connected wind energy conversion system," *Journal of Green Engineering*, vol. 6, no. 4, pp. 369-384, 2016, doi: 10.13052/jge1904-4720.642.
[14] K. Sayed, and M. Abdel-Salam, "Dynamic performance of wind turbine conversion system using PMSG-based wind simulator," *Electrical Engineering*, vol. 99, no. 1, pp. 431-439, 2017, doi: 10.1007/s00202-016-0440-z.
[15] S. Mensou, A. Essadki, I. Minka, T. Nasser, and B. B. Idrissi, "Backstepping controller for a variable wind speed energy conversion system based on a DFIG," in *2017 International Renewable and Sustainable Energy Conference (IRSEC)*, 2017, pp. 1-6, doi: 10.1109/IRSEC.2017.8477586.
[16] R. Quintal-Palomo, and M. Dybkowski, "Modelling and co-simulation of small wind turbine with permanent magnet synchronous generator," *Przegląd Elektrotechniczny*, vol. 1, no. 10, pp. 210-215, 2019, doi: 10.15199/48.2019.10.45.
[17] A. Jain, S. Shankar, and V. Vanitha, "Power generation using permanent magnet synchronous generator (PMSG) based variable speed wind energy conversion system (WECS), An overview," *Journal of Green Engineering*, vol. 7, no. 4, pp. 477-504, 2017,
[18] Y. Barradi, K. Zazi, M. Zazi, and N. Khaldi, "Control of PMSG based variable speed wind energy conversion system connected to the grid with PI and ADRC approach, "*International Journal of Power Electronics and Drive Systems (IJPEDS)*, vol. 11, no. 2, pp. 953-968, Jun. 2020, doi: 10.11591/ijpeds.v11.i2.pp953-968.
[19] M. S. Camara, M. B. Camara, B. Dakyo, and H. Gualous, "Modélisation et commande d'une génératrice synchrone à aimant permanent pour la production et l'injection des énergies offshore dans un reseau," (in French) *SGE2014, ENS Cachan*, 2014, pp. 8-10.
[20] M. Rahimi, "Modeling, control and stability analysis of grid connected PMSG based wind turbine assisted with diode rectifier and boost converter," *International Journal of Electrical Power & Energy Systems*, vol. 93, pp. 84-96, Dec. 2017, doi: 10.1016/j.ijepes.2017.05.019.
[21] E. D. Chafik, M. Hassane, and B. Anass, "A new adaptive anti-windup controller for wind energy conversion system based on PMSG," *International Journal of Power Electronics and Drive Systems (IJPEDS)*, vol. 9, no. 3, pp. 1321-1329, Sep. 2018, doi: 10.11591/ijpeds.v9.i3.pp1321-1329.
[22] H. Abid, M. Chtourou, and Ahmed Toumi "An indirect adaptive fuzzy sliding mode controller for a class of SISO nonlinear systems," *Int. J. Modelling, Identification and Control*, vol. 4, no. 2, pp. 145-159, Jan. 2008, doi: 10.1504/IJMIC.2008.021092.
[23] H. Abid, M. Chtourou, and A. Toumi, "An indirect model reference robust fuzzy adaptive control for a class of SISO nonlinear systems," *International Journal of Control, Automation, and Systems*, vol 7, no. 6, pp. 982-991, 2009, doi: 10.1007/s12555-009-0615-8.
[24] M. Mansour, M. N. Mansouri, and M. F. Mmimouni "Study and control of a variable-speed wind-energy system connected to the grid," *International Journal of Renewable Energy Research (IJRER)*, vol. 1, no. 2, pp. 96-104, 2011.
[25] T. Mitiku, and M. S. Manshahia, "Modeling of wind energy harvesting system: A systematic review," *Energy Harvesting: Modelling and Optimization of Renewable Energy Systems Using Computational Intelligence*, Apr. 2018.